



Research article

Effect of TiO₂/Fe₂O₃ nanopowder synthesis method on visible light photocatalytic degradation of reactive blue dye

Zeinab A. Suliman^{a,b,*}, Achisa C. Mecha^c, Josphat I. Mwasiagi^{a,d}^a Department of Manufacturing, Industrial and Textile Engineering, Moi University, Eldoret, Kenya^b Department of Chemical Engineering and Technology, Gezira University, Wad Madani, Sudan^c Renewable Energy, Nanomaterials and Water Research Group, Department of Chemical and Process Engineering, Moi University, Eldoret, Kenya^d Department of Technology Education, Open University of Kenya, Konza, Kenya

ARTICLE INFO

Keywords:

Photocatalysis
Reactive blue dye
Visible light
Sunlight
Titanium dioxide
Ferric oxide

ABSTRACT

Water pollution and scarcity of clean water are major issues of concern globally. In this study, titanium dioxide (TiO₂) photocatalyst doped with ferric oxide (Fe₂O₃) was used to degrade reactive blue dye (171) using sunlight irradiation. Two approaches were employed to synthesize the photocatalyst: synthesis of ferric oxide and titanium precursor through ultrasonic-assisted sol-gel method and using iron (III) nitrate nonahydrate with commercial titanium dioxide. The photocatalysts were characterized using FTIR Spectroscopy, SEM, XRD analyses, and UVDRS to determine their chemical composition, morphology, crystallinity, and light absorption, respectively. The effect of contaminant concentration (1–3 ppm), solution pH and photocatalyst type on the degradation efficiency was studied. Doping enabled visible light absorption as confirmed by the UVDRS analysis. Solar photocatalytic degradation resulted in complete (100 % removal) of the dye within 2 h under solar irradiation for all concentrations of the dye studied. Furthermore, the photocatalysts exhibited superior performance in both neutral and acidic solutions compared to basic ones. After four cycles, the dye removal efficiency has decreased by less than 15 % for all the photocatalysts confirming the significant activity and high stability of the nanocomposite. The increased dye photodegradation efficacy of Fe₂O₃ doped TiO₂ under sunlight irradiation is attributed to the narrowing of the photocatalyst's bandgap from 3.76 eV (in pure TiO₂) to 2.83 eV. This narrowing of the bandgap enhances the absorption of visible light from sunlight, thus making this photocatalyst effective under sunlight and eliminating the use of electricity which is a requirement for ultraviolet photocatalysis.

1. Introduction

There has been significant focus on reactive dyes used for dyeing and printing of cellulose fibers due to their extensive use and the need to management water effluent, so that it is discarded after pretreatment. This attention stems from the widespread detection of these dyes including reactive dyes in water discharged from the dyeing and printing factories [1]. Consequently, it is imperative to develop effective strategies for mitigating the release of these dyes into accessible water sources. Addressing this concern is vital for environmental preservation and ensuring the sustainability of water resources. Various methods, such as adsorption, biological treatment, advanced oxidation processes, and membrane technologies, have been explored for their potential to remove reactive dyes

* Corresponding author. Department of Manufacturing, Industrial and Textile Engineering, Moi University, Eldoret, Kenya.
E-mail address: zoba23165@gmail.com (Z.A. Suliman).

<https://doi.org/10.1016/j.heliyon.2024.e29648>

Received 20 November 2023; Received in revised form 25 March 2024; Accepted 11 April 2024

Available online 18 April 2024

2405-8440/© 2024 The Author(s). Published by Elsevier Ltd. This is an open access article under the CC BY-NC-ND license (<http://creativecommons.org/licenses/by-nc-nd/4.0/>).

and minimize their impact on water quality [2–4]. Photodegradation involves the decomposition of organic molecules through interaction with a photocatalyst material and exposure to UV or sun light, ultimately resulting in the production of carbon dioxide (CO₂) and water (H₂O) [2]. TiO₂ nanoparticles stand out as one of the most widely recognized photocatalysts for the breakdown of organic contaminants [5]. When exposed to UV or sun light, TiO₂ catalyzes the photodegradation process, facilitating the conversion of organic compounds into environmentally benign by-products, such as CO₂ and H₂O. This property makes TiO₂ nanoparticles highly effective in the field of photocatalysis for the removal of organic pollutants [6,7].

When the TiO₂ surface is exposed to sufficient energy that surpasses its band gap, it initiates redox reactions [8]. Subsequently, electron-hole pairs are generated, potentially instigating redox processes on the TiO₂ surface. However, the economic viability is constrained by suboptimal photoreaction rates and the limited spectral alignment between the TiO₂ absorption spectrum and solar emission spectrum. Additionally, the photocatalytic activity is hampered by rapid charge carrier recombination and sluggish charge carrier interfacial transfer rates [9–11].

Nanoparticles, including zero-valence metals, semiconductors, and certain bimetallic varieties, play a crucial role in the remediation of environmental pollutants like azo dyes, Chlorpyrifos, organochlorine pesticides, nitroaromatics, and more. Notably, metal oxide nano photocatalysts such as SiO₂, ZnO, TiO₂, Al₂O₃, Fe₂O₃ among others, are widely employed for their effectiveness. Titanium dioxide is particularly distinguished as an outstanding photocatalyst, attributed to its cost-effectiveness, non-toxicity, chemical stability, and abundance on earth [12–15]. A variety of nanomaterials have demonstrated success in removing heavy metals, organic contaminants, inorganic anions, and microorganisms. The use of nanomaterials and nanoparticles (NPs) has recently gained traction in addressing environmental challenges such as water contaminant treatment and environmental monitoring/sensing. These materials are considered advantageous due to their reactive nanostructures, which have the potential to efficiently convert and remove hazardous/toxic pollutants, transforming them into non-toxic substances [16].

Metal oxides typically exhibit a higher bandgap, rendering them particularly effective as substrate materials, especially in the UV region. This characteristic makes them well-suited for serving as a foundation in various applications. Conversely, materials with narrower bandgaps are often employed as secondary components. Notably, oxides like ZnO and TiO₂ display heightened photocatalytic activity in the UV region, making them popular choices as substrate materials in diverse applications [17]. Hematite (α-Fe₂O₃), recognized as a type band gap semiconductor with a value of 2.1 eV, has garnered significant interest due to its versatile applications. It is widely employed in various fields such as gas sensors, electrochemistry, pigments, drug carriers, and wastewater treatment. The semiconductor's distinctive properties make it valuable in sensing applications, electrochemical processes, imparting color as a pigment, serving as a carrier for pharmaceutical compounds, and effectively participating in the treatment of wastewater. The diverse range of applications which includes and not limited to dye degradation [18] and removal of organic pollutants from municipal waste water (Mecha et al., 2016) underscores hematite's importance in multiple scientific and industrial domains.

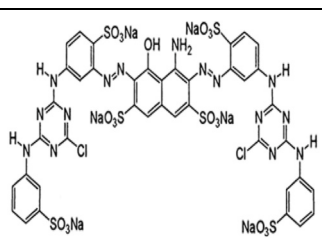
This study introduces an innovative strategy to tackle the challenge of eliminating the resilient environmental pollutant, reactive blue dye, employing advanced photocatalytic degradation processes. In contrast to traditional treatment methods that prove ineffective against emerging organic contaminants, photocatalysis effectively degrades and mineralizes the dye. The novelty of this study lies in the comparative synthesis and performance evaluation of two distinct approaches used to prepare Fe₂O₃–TiO₂ photocatalysts. Furthermore, the study contributes to knowledge by developing visible light active photocatalysts that eliminate the use of electricity which is a requirement for ultraviolet photocatalysis using pure TiO₂. It therefore makes the process environment friendly and less costly, both of which are necessary for large scale deployment of this technology in addressing water pollution.

2. Materials and methods

2.1. Materials

Titanium (IV) tetraisopropoxide 97 % (TTIP) (supplied by Aldrich), titanium dioxide (TiO₂) powder and iron (III) nitrate non-hydrate (Fe (NO₃)₃·9H₂O) (supplied by DLA company), isopropanol ((CH₃)₂CHOH, (supplied by Gelsup company), absolute ethanol (C₂H₅OH) (supplied by Eldo lab), reactive navy blue HER dyes for textile industry (supplied by Rift valley textiles (Rivatex) Ltd). The physicochemical properties of the blue dye are reported in Table 1. All the chemical reagents employed in this study were of analytical

Table 1
Physicochemical properties of Reactive Blue.

Name	Molecular Structure	Chemical Formula and structure	Molecular Formula	MW (g.mol ⁻¹)	λ max (nm) (pH = 6.0)
Reactive Blue 171	Double azo class		C ₄₀ H ₂₃ Cl ₂ N ₁₅ Na ₆ O ₁₉ S ₆	1418.93	600

grade, necessitating no additional purification.

2.2. Photocatalysts synthesis

2.2.1. Synthesis of Fe_2O_3

The method reported by Ref. [19] was used with modification. Initially, pure α - Fe_2O_3 powder was synthesized through a two-step process. Firstly, Iron III nitrate nonahydrate was dehydrated at 120 °C for 2 h, yielding the pristine material. Subsequently, this dehydrated substance underwent a controlled heat treatment at 350 °C, resulting in the production of α - Fe_2O_3 powders. To achieve the desired fine powder form, the resulting agglomerates were delicately ground using a mortar and pestle, ultimately yielding the desired α - Fe_2O_3 powder.

2.2.2. Synthesis of α - Fe_2O_3 - TiO_2 (TFT) from synthesized α - Fe_2O_3 and titanium precursor

Ultrasonic-assisted sol-gel method [20] with some modification was used. The procedure involved the dispersion of 0.2 g (equivalent to 1.25 mill moles) of α - Fe_2O_3 (synthesized in 2.2.1) in 25 mL of isopropanol through 15 min of sonication. Subsequently, this suspended solution underwent mechanical stirring, while TTIP, dissolved in 15 mL of isopropanol, was added dropwise. Following an hour of stirring, a specified amount of water was introduced, and stirring continued for an additional 2 h to ensure complete hydrolysis of TTIP. To further optimize the reaction, the mixture was subjected to 30 min of sonication in an ultrasonic cleaner. The isopropanol solvent was then removed by evaporation under reduced pressure at 50 °C using a rotary evaporator, leaving behind a precipitate, which was subsequently dried at 80 °C for 12 h and finally subjected to calcination at 350 °C for 2 h.

2.2.3. Synthesis of α - Fe_2O_3 - TiO_2 (TFC) from $Fe(NO_3)_3 \cdot 9H_2O$ and commercial TiO_2

According to Ref. [21] methods, an initial solution was prepared by dissolving iron(III) nitrate nonahydrate ($Fe(NO_3)_3 \cdot 9H_2O$) in ethanol, resulting in a solution with a concentration of 0.6 M iron nitrate. To this solution, titanium dioxide (TiO_2) powder was added while applying magnetic stirring, with the beaker covered to prevent ethanol evaporation. The solution was first stirred for 30 min, and then subjected to sonication at 35 kHz for 15 min, followed by 15 min at 130 kHz. After removing the covering film, the ethanol was evaporated overnight on a hot plate at 50 °C. The dried sample was then calcined at 300 °C for 10 min, crushed into a powder, and further heated for 6 h at 300 °C in a furnace.

2.2.4. Characterization of photocatalysts

The surface morphology of the photocatalysts was measured by the Scanning electron microscopy (SEM: Zeiss, Ultra55). The chemical composition was investigated by Fourier transform-infrared Spectroscopy (FTIR: PerkinElmer, Frontier), the samples analyzed in ATR mode (4000-650 cm^{-1}). The structure of the photocatalysts was determined using X-ray Diffraction (Model: Smartlab X-Ray Diffractometer, Tool capability: PXRD, HRXRD, XRR). Energy-dispersive X-ray analysis, EDX, was also used for the chemical analysis. The optical characteristics were examined utilizing a Shimadzu UV-3600 UV-visible spectrophotometer. To ensure accuracy, baseline correction was conducted employing a calibrated reference sample of barium sulfate. The determination of band gap (E_g) values for the photocatalysts was accomplished through the application of Equation (1) [22,23].

$$E_g = \frac{1240}{\lambda} \quad (1)$$

where: λ is the cut-off wavelength (nm) of the UV-vis absorption spectra.

2.3. Degradation of reactive blue dye under visible light irradiation

Photodegradation studies were conducted using three distinct concentrations of Reactive Navy Blue HER dye (1, 2, 3 ppm) and pH = 7. In individual 20 ml test tubes, 0.02 mg of Fe_2O_3 - TiO_2 was introduced, followed by the addition of the respective concentrations of the blue dye. Subsequently, the test tubes were positioned under direct sunlight irradiation. Samples were collected within a period of 2 h and the concentration of the dye was determined using UV-visible spectroscopy at $\lambda_{max} = 600$ nm to see the effect of the initial concentration of the dye and irradiation time.

To observe the impact of pH variations, samples of a 1 ppm dye solution were prepared under different pH conditions—acidic at pH 3, neutral at pH 7, and alkaline at pH 11. Subsequently, all samples were subjected to identical conditions for analysis.

The photocatalyst degradation efficiency was evaluated as the removal percentage of Reactive blue dye, equation (2)

$$\text{Removal Efficiency (\%)} = \frac{C_0 - C_t}{C_0} \times 100\% \quad (2)$$

where: C_0 and C_t represent the initial and final concentrations of Reactive blue dye by (ppm) respectively.

2.4. The effect of the pH

The dye removal rate is significantly influenced by the pH of the test solution. In this investigation, 20 ml of a blue dye solution with a concentration of 1 mg/L was utilized. To manipulate the pH within the range of 3–11, precise amounts of HCl and NaOH 0.1 M

solutions were added. Subsequently, 0.004 g/L of each photocatalyst was introduced separately into each container. The solutions were then exposed to a sun light irradiation for 60 min for half of them and 120 min for the remainder. Afterward, the specimens were separated and filtered, and the absorbance of each solution was measured using a spectrophotometer. This absorbance data was then compared with the initial absorption levels before undergoing the photocatalytic process.

2.5. Photocatalyst reusability and stability

The evaluation of nanophotocatalyst performance in extensive applications and the economic efficiency of the photo degradation process rely on key factors like robust stability and a simple recovery process. This specific investigation focuses on the $\text{Fe}_2\text{O}_3\text{-TiO}_2$ nanophotocatalyst, with a notable feature being the absence of any chemical treatment for removing pollutants from its surface. Instead, the methodology involves allowing the solution to settle for several hours, followed by water separation and concluding with a drying process at 60 °C, as reported by Ref. [24] methods.

3. Results and discussion

3.1. Photocatalysts characterization

3.1.1. XRD analysis

The X-ray diffraction (XRD) analysis results are shown in Fig. 1. A total of eleven well-defined peaks, all of which can be attributed to the $\alpha\text{-Fe}_2\text{O}_3$ phase, commonly known as hematite were observed. The prominent peaks were detected at angles of 24.9, 33.27, 35.39, 41.103, 48.2, 53.9, 57.4, 62.2, 63.8, 71.82, and 75.9°, corresponding to the respective diffraction planes (012), (104), (110), (113), (024), (116), (122), (214), (300), (1010), and (220) of hematite [25,26]. Furthermore, the presence of two additional peaks at 25.1 and 48.2°, corresponding to the diffraction planes (101) and (200), indicated the presence of the TiO_2 anatase phase within the sample [20, 27].

The average crystallite size of the photocatalysts was determined using the Debye–Scherrer equation as reported in Table 2. In this equation, d represents the crystallite size, λ stands for the wavelength of the incident X-ray, β is the full width at half maximum (FWHM) of the diffraction formula, K is the Scherrer constant (a typical value is 0.94), and θ represents the scattering angle.

The Debye–Scherrer equation is given by:

$$d = \frac{K\lambda}{\beta \cos \theta}$$

3.1.2. FTIR analysis

The FTIR spectra of the synthesized $\text{TiO}_2\text{-Fe}_2\text{O}_3$ photocatalysts from the commercial and synthesized TiO_2 and the Fe_2O_3 , between 400 and 4000 cm^{-1} is shown in Fig. 2. The spectra exhibited distinctive peak patterns at 1074 cm^{-1} , 1630 cm^{-1} , and 3439 cm^{-1} , which are indicative of the presence of $\text{TiO}_2\text{-Fe}_2\text{O}_3$ in the material. The broader peaks observed at 3439 cm^{-1} and 1620 cm^{-1} are attributed to -OH stretching and bending vibrations and are likely to play a significant role in phase formation and stabilization across all nanocomposites. The peak at 1074 cm^{-1} can be attributed to C-O stretching vibration, while the strong band below 700 cm^{-1} is associated with the Fe-O stretching mode. Specifically, the Fe-O stretching mode is observed at 556 cm^{-1} and 471 cm^{-1} in pure Fe_2O_3 and in commercial TiO_2 doped with Fe_2O_3 [28,29], but in the $\text{TiO}_2\text{-Fe}_2\text{O}_3$ nanocomposite synthesized from precursor materials, it appears as a single stretching peak. Furthermore, a broad band in the 500-600 cm^{-1} range is linked to the vibration of the Ti-O bonds [30].

3.1.3. SEM analysis

The surface morphology of iron oxide analyzed using SEM is depicted in Fig. 3 The SEM images reveal an agglomerated shape

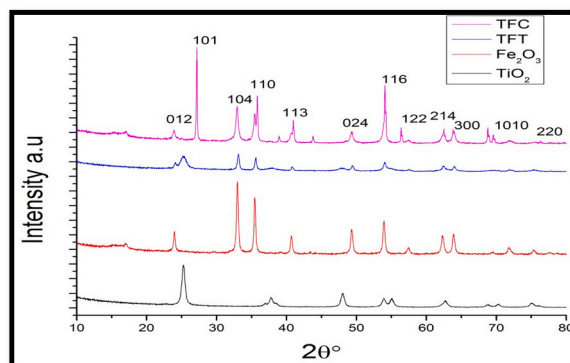
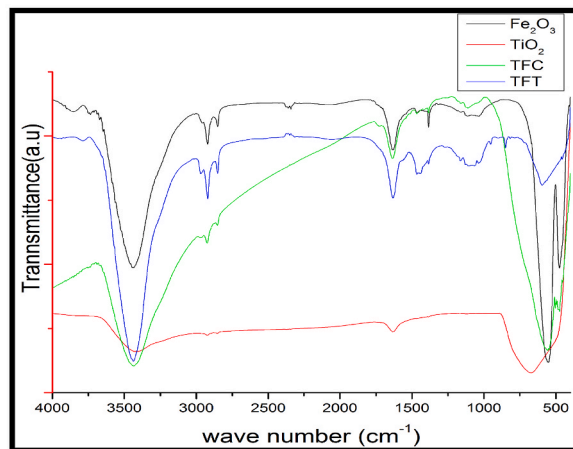
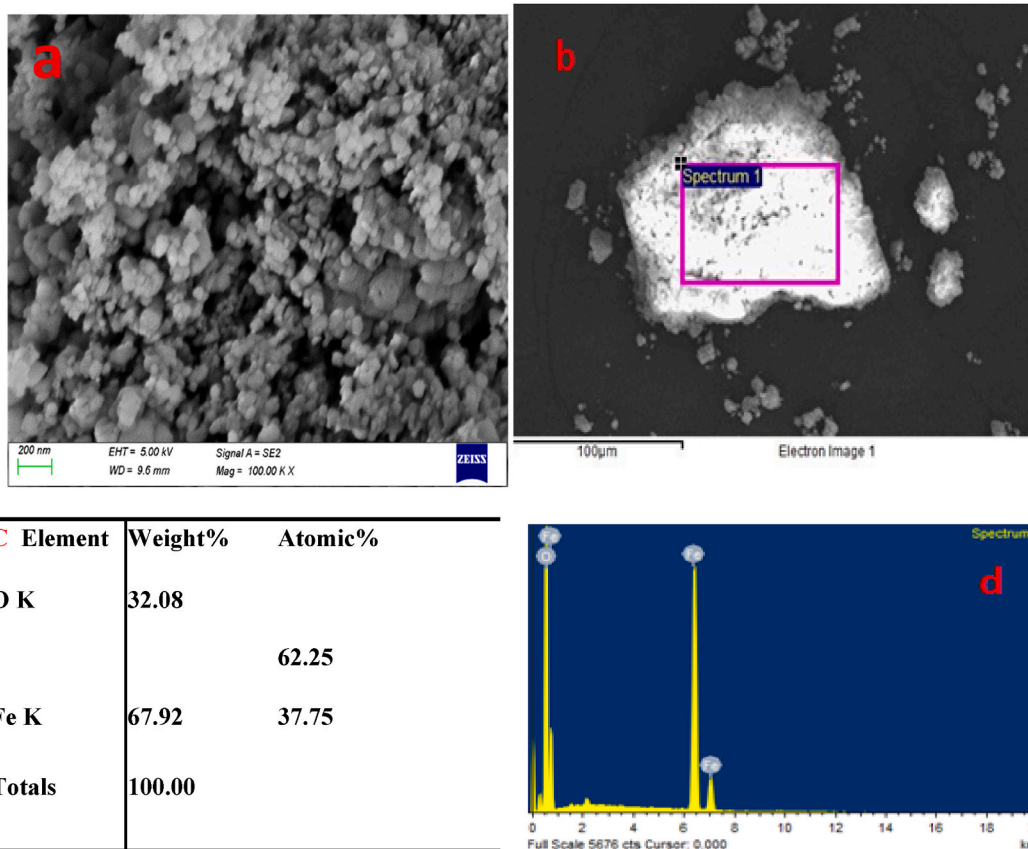


Fig. 1. XRD curves of $\alpha\text{-Fe}_2\text{O}_3$ nanopowder, TiO_2 photocatalyst, doping TFT and TFC photocatalysts.

Table 2

Crystals size of the photocatalysts.

Photocatalyst type	TiO ₂	Fe ₂ O ₃	TFC	TFT
Crystal size	14.83	22.54	38.2	32.3

Fig. 2. FTIR curves of α -Fe₂O₃ nanopowder, TiO₂ photocatalyst, doping TFT and TFC photocatalysts.Fig. 3. (a) SEM images 100.00 K X magnification and (b, c, and d) EDX images of synthesis Fe₂O₃ nonparticles

morphology, indicating that the nanoparticles exhibit a tendency to cluster and form larger assemblies due to their elevated surface energies [10]. The EDX analysis confirms the precise composition of the iron oxide, with 67.92 % iron content and 32.8 % oxygen content, highlighting the successful preparation of the material.

Fig. 4 displays SEM images of the photocatalyst synthesized from the combination of Fe_2O_3 and a titanium precursor. The images reveal a somewhat porous and agglomerated morphology in the sample, suggesting potential advantages for property enhancement. Notably, both large and small particles of nearly equal sizes were observed in the images [28]. The confirmation of elemental composition in the composites was carried out through EDX measurements, providing a comprehensive understanding of the synthesized photocatalyst's constituent elements.

Surface morphology analysis was conducted on commercially available TiO_2 nanoparticles doped with synthesized iron oxide. The SEM images in Fig. 5 of the Fe_2O_3 -doped TiO_2 , revealing a distinctive spherical shape morphology on the nanoparticle surface. At a magnification of 100,000 times, a denser distribution of spherical shapes with minimal empty spaces is evident, Furthermore, Fig. 5 illustrates the occurrence of agglomeration of these spherical shapes, forming clusters within the samples [31].

The findings indicate that the particle size of the photocatalyst synthesized from the Titanium precursor is smaller compared to that of commercially available Titanium, as depicted in Figs. 4 and 5. The results suggest that an escalation in calcination time leads to heightened material crystallinity. However, it is noteworthy that elevating the calcination time might concurrently result in an increase in crystal grain size.

3.1.4. UV-DRS analysis

Fig. 6 illustrates the UV-visible diffuse reflectance spectra (DRS) for $\alpha\text{-Fe}_2\text{O}_3$, TiO_2 , and the two synthesized $\alpha\text{-Fe}_2\text{O}_3\text{-TiO}_2$ powders. The pristine $\alpha\text{-Fe}_2\text{O}_3$ powder displays broad absorption across the entire UV-visible spectrum, displays photo-absorption about 527 nm, corresponding to band-gap energy of 2.35 eV. In contrast, $\text{TiO}_2/\text{Fe}_2\text{O}_3$ photocatalysts exhibit extensive optical absorption in both the UV and visible ranges, displays photo-absorption about 438.8 nm, corresponding to band-gap energy of 2.83 eV. While pristine TiO_2 powder only demonstrates limited absorption in the UV range. TiO_2 specifically displays photo-absorption in the UV-light region below 400 nm, corresponding to band-gap energy of 3.76 eV. Notably, the optical absorptions of the $\alpha\text{-Fe}_2\text{O}_3/\text{TiO}_2$ composites exhibit a noticeable red-shift in the visible light region compared to TiO_2 , attributed to the presence of $\alpha\text{-Fe}_2\text{O}_3$ in the composite powders. This observation suggests that $\alpha\text{-Fe}_2\text{O}_3/\text{TiO}_2$ composites could serve as effective photocatalysts for utilizing sunlight as an energy source for contaminant reduction [19].

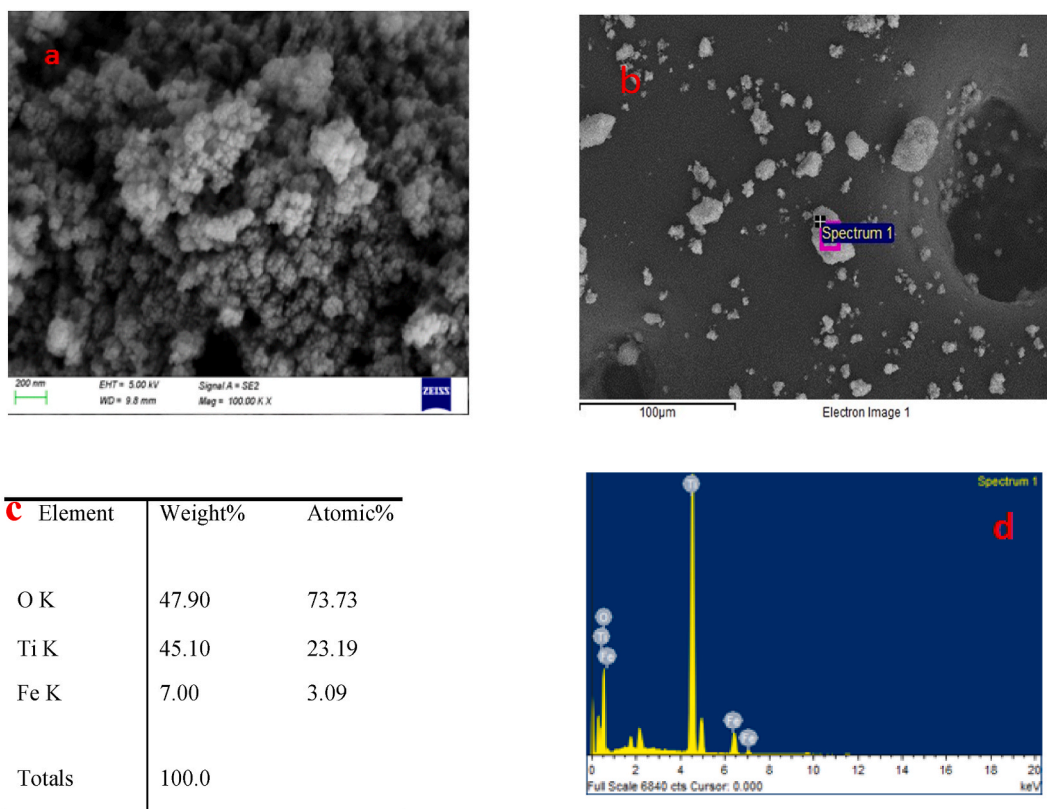


Fig. 4. (a) SEM images 100.00 K X magnification and (b, c, and d) EDX images of $\alpha\text{-Fe}_2\text{O}_3\text{-TiO}_2$ (TFT) from Synthesis Fe_2O_3 and titanium precursor.

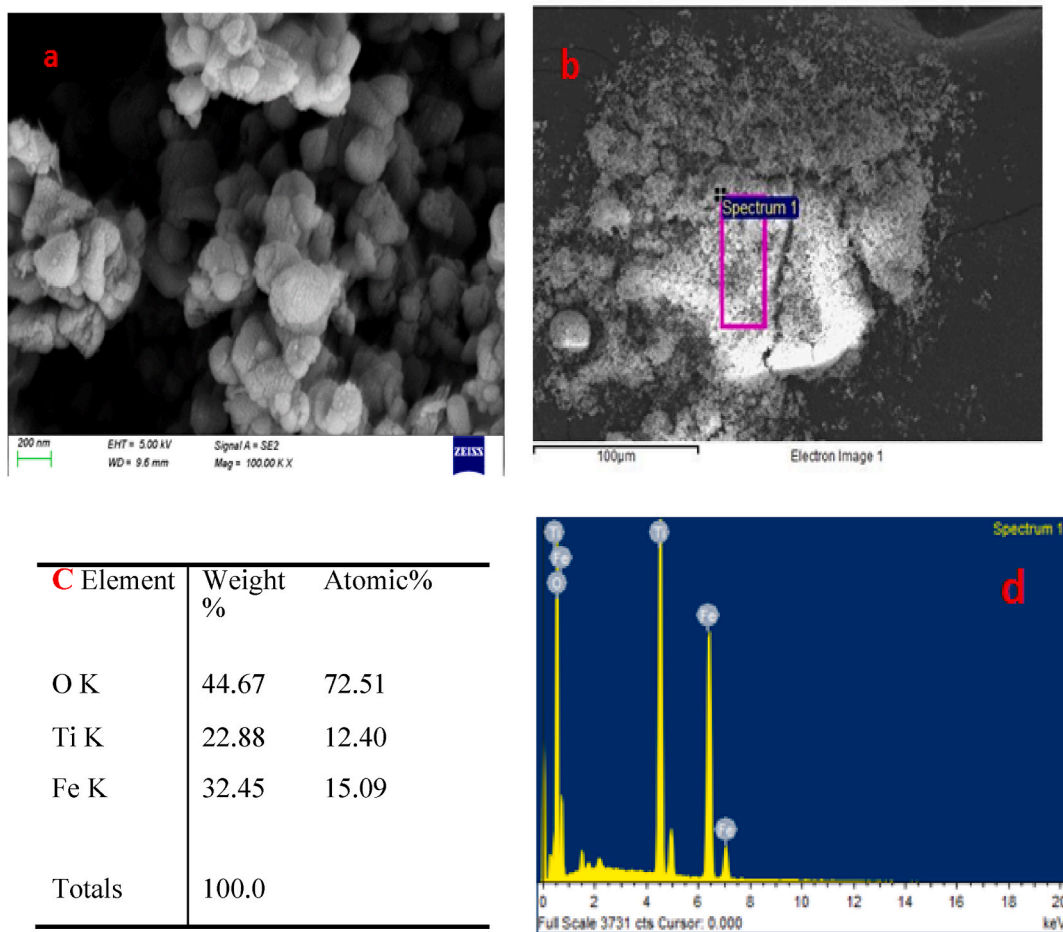


Fig. 5. (a) SEM images 100.00 K X magnification and (b, c, and d) EDX images of α -Fe₂O₃-TiO₂ (TFC) from Fe (NO₃)₃ 9H₂O and commercial TiO₂.

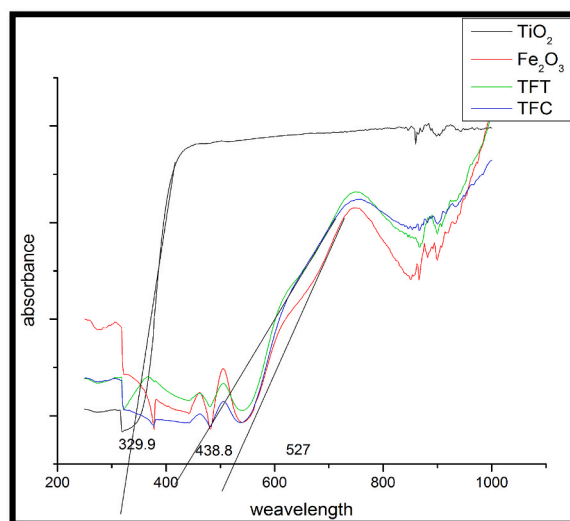
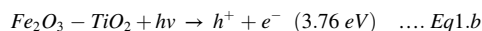


Fig. 6. UV DRS curves of α -Fe₂O₃ nanopowder, TiO₂ photocatalyst, doping TFT and TFC photocatalysts.

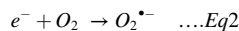
3.2. Degradation of reactive blue dye under visible light irradiation

3.2.1. Degradation mechanism

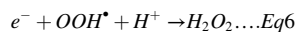
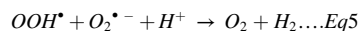
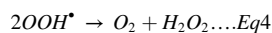
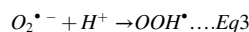
When the blue dye solution is exposed to the sun light, photon energy ($h\nu$) higher than the bandgap is absorbed by the materials (typically with the ultraviolet illumination). Excited electrons move to the conduction band. Holes are the positively charge carriers that remain in the valence band after it has been filled as shown in Eq. (1).a &1.b [32].



The division of photogenerated electrons and holes is displayed in the following phase (Eq (2)) [33].



The optimum end products of a photocatalytic reaction, like those of other AOPs, are CO_2 and water. Electron acceptors use the electrons in the conduction band as countercharge carriers, while hydroxyl groups or organic compounds consume the holes. Given that it results in the creation of additional reactive oxygen species, dissolved oxygen (DO) serves as a primary electron acceptor. Its presence is essential to maintain the electron-hole separation and to facilitate photocatalysis as DO reacts with electrons. As illustrated in Eq. 3–9 [32].



3.2.2. The effect of initial concentration of the dye with the time of irradiation

The evaluation of the photocatalytic organic degradation of the blue dye using several concentration of the dye (1, 2 and 3 ppm) on different irradiation time was conducted and the results are illustrated in Table S1 (supplementary materials), Fig (7)–(9) The doped TiO_2 exhibited superior removal efficiency in eliminating the blue dye compared to pure TiO_2 , achieving a 100 % removal percentage after 2 h of sun light irradiation for both photocatalysts.

3.2.3. The effect of pH

The resulting removal percentages were plotted as a function of pH in the 3–11 range, as illustrated in Fig.(10)–(12), and Table S2 (supplementary materials).

The degradation of Reactive Blue 171 dye was found to be more effective in acidic and neutral pH ranges when utilizing bare TiO_2 or codoped photocatalysts ($\text{TiO}_2\text{-Fe}_2\text{O}_3$). This observation can be attributed to the point of zero net charge (PZC) of the photocatalysts,

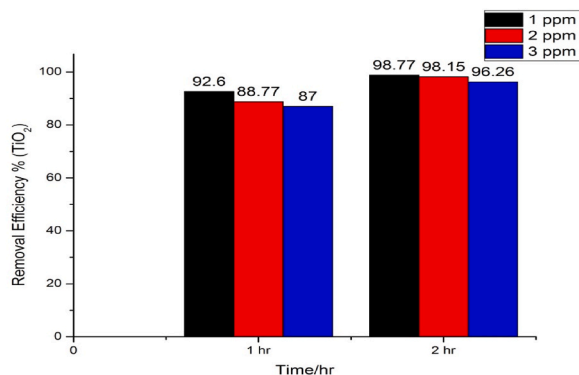


Fig. 7. Removal efficiency % of blue dye using TiO_2 photocatalyst: Concentration of dye Vs. Time. (For interpretation of the references to color in this figure legend, the reader is referred to the Web version of this article.)

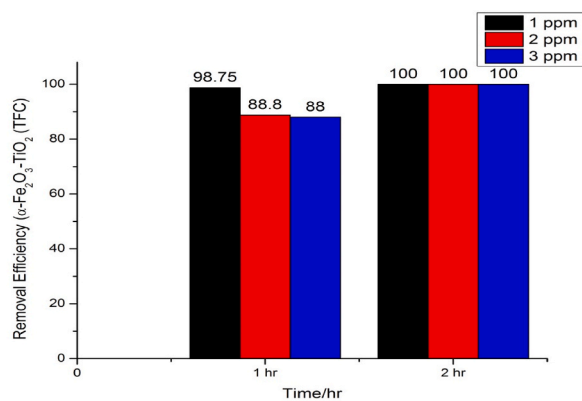


Fig. 8. Removal efficiency % of blue dye using $\alpha\text{-Fe}_2\text{O}_3\text{-TiO}_2$ (TFC) photocatalyst: Concentration of dye Vs. Time. (For interpretation of the references to color in this figure legend, the reader is referred to the Web version of this article.)

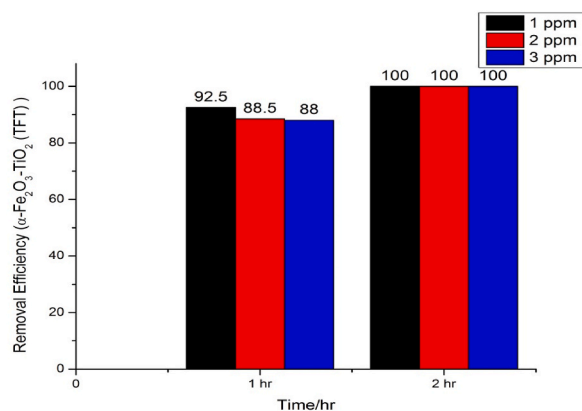


Fig. 9. Removal efficiency %/hr of blue dye using $\alpha\text{-Fe}_2\text{O}_3\text{-TiO}_2$ (TFT) photocatalyst: Concentration of dye Vs. Time. (For interpretation of the references to color in this figure legend, the reader is referred to the Web version of this article.)

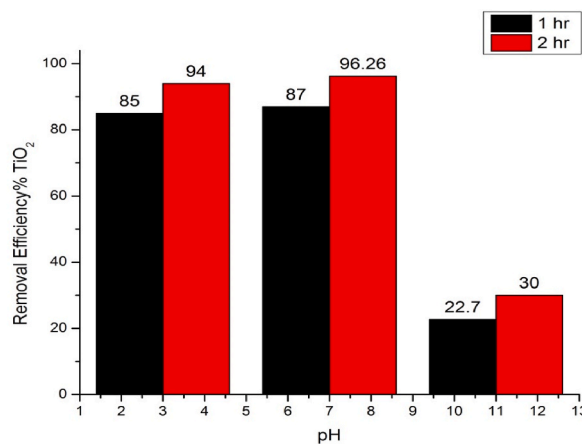


Fig. 10. Removal Efficiency % of TiO_2 Vs. pH within 1 and 2 h irradiation time.

which is at pH 6.8. In an acidic solution ($\text{pH} < 6.8$), the photocatalysts carry a positive charge, while Reactive Blue 171 exhibits a negative charge due to the sulfonic group present. This favorable electrostatic interaction promotes the adsorption of the anionic Reactive Blue 171 dye onto the surface of the photocatalyst.

In this scenario, the positively charged photocatalysts actively attract and adsorb more dye molecules onto its active sites,

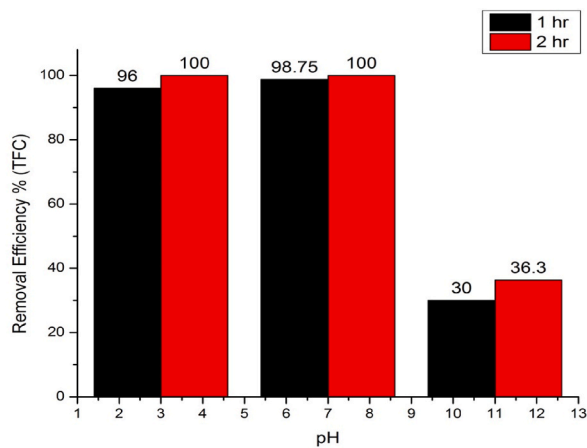


Fig. 11. Removal Efficiency % of TFC Vs. pH within 1 and 2 h irradiation time.

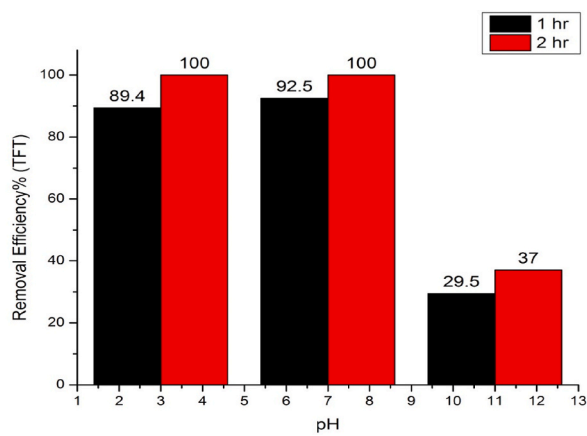


Fig. 12. Removal Efficiency % of TFT Vs. pH within 1 and 2 h irradiation time.

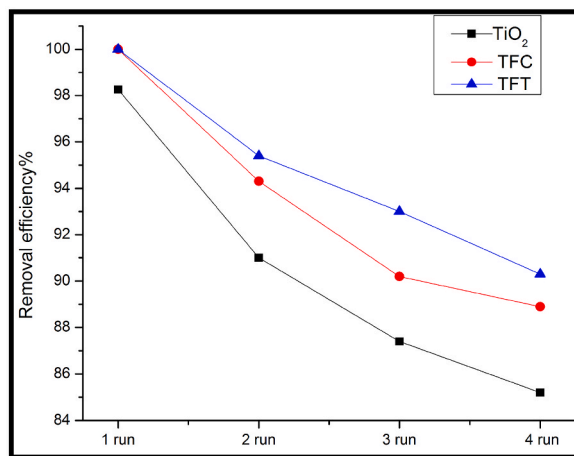


Fig. 13. The obtained results from the evaluation of the stability and activity of 1 ppm initial dye concentration in TiO₂, TFC, and TFT in 20 ml solution up to 4 consecutive cycles.

leading to an enhancement in the degradation efficiency of Reactive Blue 171. Previous literature has also linked photocatalytic activity with the adsorption of dye molecules onto the surface of photocatalysts, as reported by Refs. [3,24,34,35].

At elevated pH levels, photocatalysts assume a negative charge as the pH surpasses the point of zero net charge (PZC). The repulsion between the negatively charged photocatalysts and the similarly negatively charged dye molecules impedes the adhesion of dye molecules to the catalyst surface. Consequently, the photodegradation process becomes more challenging, as the degradation facilitated by electron-hole pairs ($h\nu$) and conduction-band electrons (e_{CB}) is obstructed. The hydroxyl radicals generated by the photocatalysts play a crucial role in degrading dye molecules. However, in alkaline conditions, the presence of OH^- interrupts the photodegradation process. This interruption occurs because OH^- induces the formation of intramolecular hydrogen bonds in electron-donating groups, such as $^-NH_2$ located in the α -position of the carbonyl group of Reactive Blue 171. This leads to increased chemical stability of the dye, making it more resistant to attack by hydroxyl radicals. Consequently, a decrease in photocatalytic activity is observed in alkaline solutions due to these hindrances in the degradation process. This effect has been previously documented, as reported by Ref. [3].

3.2.4. The stability & Reusability of nanophotocatalysis

The findings of the study, presented in Fig. 11, provide insights into the stability and activity of the photocatalyst over four consecutive cycles. This emphasizes the practical importance of understanding how well the catalyst maintains stability and efficacy across multiple usage instances, offering valuable insights into its suitability for large-scale applications with economic and environmental considerations. Notably, the results in Fig. 13 indicate that after the fourth cycle, the reactive blue dye removal efficiency has only decreased by about 13.06 % for bare TiO_2 and 11.1 % for $Fe_2O_3-TiO_2$ (TFC), and 9.7 % for $Fe_2O_3-TiO_2$ (TFT) a confirming the significant activity and high stability of the $Fe_2O_3-TiO_2$ nanocomposite.

3.2.5. Comparison of bare and doped TiO_2 nanophotocatalysts with other nanophotocatalysts

The TiO_2 nanophotocatalyst stands out as a unique semiconductor with excellent photodegradation activity. While TiO_2 typically requires a UV source or doping with metal or metal oxide to effectively absorb sunlight irradiation as reported by Ref. [36], even a concentration of 0.02 g/L of TiO_2 demonstrates significant efficiency, removing 96.26 % of a 1 mg/L dye solution under sunlight irradiation. Moreover, the introduction of Fe_2O_3 through doping enhances its performance, achieving 100 % removal efficiency after 120 min of sunlight irradiation. Table .3 compiles findings from various studies exploring nanoparticle applications for organic dye removal in wastewater. Notably, codoped TiO_2 emerges as the most promising option, offering the highest removal efficiency. Its ability to operate under sunlight irradiation is a key advantage, contributing to cost reduction and utilizing clean energy sources.

4. Conclusion

In this study $\alpha-Fe_2O_3$ and $\alpha-Fe_2O_3-TiO_2$ from commercial TiO_2 and from syntheses TiO_2 were synthesis successfully as the characterization result proved. The hematite iron oxide nanoparticles, synthesized through the Sol-Gel method, were identified as such through X-ray diffraction (XRD) analysis. Scanning electron microscopy (SEM) revealed flowered structures, confirming the presence of iron oxide. Further confirmation of iron oxide and identification of functional groups were established through Fourier-transform infrared spectroscopy (FTIR). Additionally, the optical properties of the nanoparticles were investigated using UV diffuse reflectance spectroscopy (UV DRS). Metal doping enhances the optical properties of TiO_2 thus enabling utilization of solar light for photocatalysis as it appear in the UV DRS curves. There were no significant changes in the characteristics of the photocatalysts preparing by the commercial TiO_2 than the synthesis TiO_2 in the FTIR and the XRD results, and they absorbed in the same wavelength in the UV DRS. While their morphology was little bit different as the SEM images showed, the photocatalytic synthesis from the titanium precursor had a smaller grains size and it tended to agglomerate and make clusters more than the one created from the commercial TiO_2 , and also the percentage of titanium in the $\alpha-Fe_2O_3-TiO_2$ photocatalysts from TiO_2 precursor more than the titanium in the $\alpha-Fe_2O_3-TiO_2$

Table 3

Comparison of various nanophotocatalysts for the removal of organic dyes considering the source of light and experimental conditions.

Nanophotocatalytic type	Photocatalytic Dosage ($g L^{-1}$)	t (min)	Pollutant	Source of light	Removal/efficiency (%)	Ref.
Anatase Nano- TiO_2	1	40	Reactive Blue 4	125 W UV lamp/ sun light	100	[3]
N-Cu, N-Fe and N codoped TiO_2 and Bare TiO_2	0.06	5	RB 4 dye	100 W halogen lamp	100, 84, 80 and 75	[37]
TiO_2	1	120	Procion Navy H-EXL (PN)	UV-LED	100	[38]
$CoAl_2O_4$	0.25	150	navy blue	UVA lamps 75Watts	42–67	[39]
ZnO	0.01–0.06	20	reactive blue 203	8W UV lamp	99.1	[2]
TiO_2 , Fe_2O_3 and $TiO_2-Fe_2O_3$	60	60	Titan Yellow and Methyl Orange	UV lamp	92.98, 71.67 and 62.89 % for TY	[28]
$Cu_2SnS_3 + GO$	0.4	240	Navy Blue ME2RL	300 W xenon lamp	88	[40]
Bare TiO_2 and $TiO_2-Fe_2O_3$	0.004	120	Navy Blue 171	Sun light	96.26 and 100	This work

photocatalysts from commercial TiO₂ confirmed by the EDX, The two photocatalysts exhibited impressive efficiency, achieving a complete elimination of the blue dye after 2 h of exposure to sunlight across different concentrations. Notably, these photocatalysts outperformed in both neutral (96.26 %, 100 %, and 100 %) and acidic (94 %, 100 %, and 100 %) solutions compared to basic conditions (30 %, 36.3 %, and 37 %) for TiO₂, commercially doped TiO₂, and synthesized doped TiO₂. Even after four cycles, the reduction in dye removal efficiency was less than 15 % for all photocatalysts, confirming the substantial activity and enduring stability of the nanocomposite.

Data availability statement

Data will be made available on request.

Additional information

Additional information is available on the supplementary materials.

CRediT authorship contribution statement

Zeinab A. Suliman: Writing – review & editing, Writing – original draft, Visualization, Validation, Formal analysis, Data curation. **Achisa C. Mecha:** Writing – review & editing, Visualization, Supervision, Conceptualization. **Josphat I. Mwasiagi:** Writing – review & editing, Visualization, Supervision, Conceptualization.

Declaration of competing interest

The authors declare the following financial interests/personal relationships which may be considered as potential competing interests: Zeinab A. Suliman reports financial support was provided by European Commission. None If there are other authors, they declare that they have no known competing financial interests or personal relationships that could have appeared to influence the work reported in this paper.

Acknowledgement

The authors thank the European commission (EU) for funding this study through Strengthening mobility and promoting Regional Integration in Engineering Education in Africa (SPREE) program (Grant numbers 614586-mobaf-20191-1).

Appendix A. Supplementary data

Supplementary data to this article can be found online at <https://doi.org/10.1016/j.heliyon.2024.e29648>.

References

- [1] M. Siddique, R. Farooq, A. Shaheen, Removal of Reactive Blue 19 from wastewaters by physicochemical and biological processes-a review, *J. Chem. Soc. Pakistan* 33 (2011).
- [2] M. Bagheri, N.R. Najafabadi, E. Borna, Removal of reactive blue 203 dye photocatalytic using ZnO nanoparticles stabilized on functionalized MWCNTs, *J. King Saud Univ. Sci.* 32 (1) (2020) 799–804.
- [3] E.M. Samsudin, et al., Evaluation on the photocatalytic degradation activity of reactive blue 4 using pure anatase nano-TiO₂, *Sains Malays.* 44 (7) (2015) 1011–1019.
- [4] M. Behera, et al., A review on the treatment of textile industry waste effluents towards the development of efficient mitigation strategy: an integrated system design approach, *J. Environ. Chem. Eng.* 9 (4) (2021) 105277.
- [5] C. Wang, et al., Improved photocatalytic oxidation performance of gaseous acetaldehyde by ternary g-C₃N₄/Ag-TiO₂ composites under visible light, *J. Colloid Interface Sci.* 602 (2021) 699–711.
- [6] D. Jagadeesan, et al., Hollow spheres to nanocups: tuning the morphology and magnetic properties of single-crystalline α -Fe₂O₃ nanostructures, *Angew. Chem.* 120 (40) (2008) 7799–7802.
- [7] A. Bee, R. Massart, S. Neveu, Synthesis of very fine maghemite particles, *J. Magn. Magn. Mater.* 149 (1–2) (1995) 6–9.
- [8] F.S. Arghavan, et al., Complete degradation of tamoxifen using FeNi₃@ SiO₂@ ZnO as a photocatalyst with UV light irradiation: a study on the degradation process and sensitivity analysis using ANN tool, *Mater. Sci. Semicond. Process.* 128 (2021) 105725.
- [9] M. Mohsenzadeh, S.A. Mirbagheri, S. Sabbaghi, Photocatalytic degradation of 1, 2-dichloroethane using immobilized PAni-TiO₂ nanocomposite in a pilot-scale packed bed reactor, *Desalination Water Treat.* 155 (2019) 72–83.
- [10] S.H. Gurlhosur, B. Sreekanth, Synthesis, characterization of iron oxide (α -Fe₂O₃) nanoparticles and its application in photocatalytic reduction of chromium (VI), *Rasayan Journal of Chemistry* 11 (4) (2018) 1678–1685.
- [11] S. Peiris, et al., Recent development and future prospects of TiO₂ photocatalysis, *J. Chin. Chem. Soc.* 68 (5) (2021) 738–769.
- [12] A.A. Yaqoob, et al., Role of nanomaterials in the treatment of wastewater: a review, *Water* 12 (2) (2020) 495.
- [13] K. Umar, et al., Synthesis, characterization of Mo and Mn doped ZnO and their photocatalytic activity for the decolorization of two different chromophoric dyes, *Appl. Catal. Gen.* 505 (2015) 507–514.
- [14] B. Bhanvase, T. Shende, S. Sonawane, A review on graphene-TiO₂ and doped graphene-TiO₂ nanocomposite photocatalyst for water and wastewater treatment, *Environmental Technology Reviews* 6 (1) (2017) 1–14.

- [15] K.L. Seneviratne, et al., Recent progress in visible-light active (VLA) TiO₂ nano-structures for enhanced photocatalytic activity (PCA) and antibacterial properties: a review, *Iran. J. Catal.* 11 (3) (2021) 217–245.
- [16] M. Nasrollahzadeh, et al., Green-synthesized nanocatalysts and nanomaterials for water treatment: current challenges and future perspectives 401 (2021) 123401.
- [17] U.Q. Satti, et al., Simple two-step development of TiO₂/Fe₂O₃ nanocomposite for oxygen evolution reaction (OER) and photo-bio active applications, *Colloids Surf. A Physicochem. Eng. Asp.* 671 (2023) 131662.
- [18] A. Abbasi, et al., Photo-degradation of methylene blue: photocatalyst and magnetic investigation of Fe₂O₃-TiO₂ nanoparticles and nanocomposites, *J. Mater. Sci. Mater. Electron.* 27 (2016) 4800–4809.
- [19] A. Bouziani, J. Park, A. Ozturk, Synthesis of α -Fe₂O₃/TiO₂ heterogeneous composites by the sol-gel process and their photocatalytic activity, *J. Photochem. Photobiol. Chem.* 400 (2020) 112718.
- [20] A.-M. Abdel-Wahab, et al., Photocatalytic degradation of paracetamol over magnetic flower-like TiO₂/Fe₂O₃ core-shell nanostructures, *J. Photochem. Photobiol. Chem.* 347 (2017) 186–198.
- [21] E. Ahmadi, et al., Synergistic effects of α -Fe₂O₃-TiO₂ and Na₂S₂O₈ on the performance of a non-thermal plasma reactor as a novel catalytic oxidation process for dimethyl phthalate degradation, *Separ. Purif. Technol.* 250 (2020).
- [22] A.B. Jasso-Salcedo, G. Palestino, V.A. Escobar-Barrios, Effect of Ag, pH, and time on the preparation of Ag-functionalized zinc oxide nanoagglomerates as photocatalysts, *J. Catal.* 318 (2014) 170–178.
- [23] A.C. Mecha, et al., UV and solar light photocatalytic removal of organic contaminants in municipal wastewater, *Separ. Sci. Technol.* 51 (10) (2016) 1765–1778.
- [24] M. Najafi, et al., Sono-sorption versus adsorption for the removal of Congo red from aqueous solution using NiFeLDH/Au nanocomposite: kinetics, thermodynamics, isotherm studies, and optimization of process parameters, *J. Ind. Eng. Chem.* 116 (2022) 489–503.
- [25] H.M. Asoufi, T.M. Al-Antary, A.M. Awwad, Green route for synthesis hematite (α -Fe₂O₃) nanoparticles: toxicity effect on the green peach aphid, *Myzus persicae* (Sulzer), *Environ. Nanotechnol. Monit. Manag.* 9 (2018) 107–111.
- [26] A. Lassoued, et al., Synthesis, photoluminescence and Magnetic properties of iron oxide (α -Fe₂O₃) nanoparticles through precipitation or hydrothermal methods, *Phys. E Low-dimens. Syst. Nanostruct.* 101 (2018) 212–219.
- [27] H. Jladpanah-Saravy, et al., Synthesis of titanium dioxide nanoparticles for photocatalytic degradation of cyanide in wastewater, *Anal. Lett.* 47 (10) (2014) 1772–1782.
- [28] M.A. Kumar, et al., Enhanced photocatalytic and electrochemical performance of TiO₂-Fe₂O₃ nanocomposite: its applications in dye decolorization and as supercapacitors, *Sci. Rep.* 10 (1) (2020) 1249.
- [29] A. Dehbi, et al., Hematite iron oxide nanoparticles (α -Fe₂O₃): synthesis and modelling adsorption of malachite green, *J. Environ. Chem. Eng.* 8 (1) (2020) 103394.
- [30] S. Talebi, N. Chaibakhsh, Z. Moradi-Shoeili, Application of nanoscale ZnS/TiO₂ composite for optimized photocatalytic decolorization of a textile dye, *J. Appl. Res. Technol.* 15 (4) (2017) 378–385.
- [31] P. Gareso, et al., Synthesis and material characterization of TiO₂ nanoparticles doped with iron (Fe), in: *Journal of Physics: Conference Series*, IOP Publishing, 2021.
- [32] H.N. Le, A Concept for Nanoparticle-Based Photocatalytic Treatment of Wastewater from Textile Industry, Hanoi University of Science and Technology, 2018.
- [33] S. Sharma, S.K. Mehta, S.K. Kansal, N doped ZnO/C-dots nanoflowers as visible light driven photocatalyst for the degradation of malachite green dye in aqueous phase, *J. Alloys Compd.* 699 (2017) 323–333.
- [34] N. Daneshvar, D. Salari, A. Khataee, Photocatalytic degradation of azo dye acid red 14 in water: investigation of the effect of operational parameters, *J. Photochem. Photobiol. Chem.* 157 (1) (2003) 111–116.
- [35] A. Aguedach, S. Brosillon, J. Morvan, Photocatalytic degradation of azo-dyes reactive black 5 and reactive yellow 145 in water over a newly deposited titanium dioxide, *Appl. Catal. B Environ.* 57 (1) (2005) 55–62.
- [36] V. Mahmoodi, T.R. Bastami, A. Ahmadpour, Solar energy harvesting by magnetic-semiconductor nanoheterostructure in water treatment technology, *Environ. Sci. Pollut. Control Ser.* 25 (2018) 8268–8285.
- [37] N. Kaur, S.K. Shahi, V. Singh, Anomalous behavior of visible light active TiO₂ for the photocatalytic degradation of different Reactive dyes, *Photochem. Photobiol. Sci.* 14 (2015) 2024–2034.
- [38] T. Tapia-Tlatelpa, J. Trull, L. Romeral, In situ decolorization monitoring of textile dyes for an optimized UV-LED/TiO₂ reactor, *Catalysts* 9 (8) (2019) 669.
- [39] Y. El Jabbar, et al., Photocatalytic degradation of navy blue textile dye by nanoscale cobalt aluminate prepared by polymeric precursor method, *Environ. Nanotechnol. Monit. Manag.* 12 (2019) 100259.
- [40] H.D. Shelke, et al., Enhanced photocatalytic activity of the Cu₂SnS₃+ GO composite for the degradation of navy blue ME2RL industrial dye, *Coatings* 13 (3) (2023) 522.